AGU100 ADVANCING EARTH AND SPACE SCIENCE

Geochemistry, Geophysics, Geosystems

RESEARCH ARTICLE

10.1029/2017GC007369

Constraining the Timing and Amplitude of Early Serpukhovian Glacioeustasy With a Continuous Carbonate Record in Northern Spain

Alison Campion[1], Adam Maloof[1], Blair Schoene[1], Sergey Oleynik[1], Javier Sanz-López[2], Silvia Blanco-Ferrera[2], Oscar Merino-Tomé[2], Juan Ramón Bahamonde[2], and Luis Pedro Fernández[2]

[1]Department of Geosciences, Princeton University, Princeton, NJ, USA, [2]Departmento de Geologia, Universidad de Oviedo c/Jesús Arias de Velasco s/n, Oviedo, Spain

Key Points:
- Mid-Carboniferous Spanish limestones were not subaerially exposed and may offer an approximation of $\delta^{13}C$ of oceanic DIC
- An increase in $\delta^{13}C$ of oceanic DIC can be explained by widespread meteoric diagenesis of subaerially exposed carbonate basins
- Major eustatic fall due to LPIA glacial advance began at 330 Ma and lasted for ~3.5My

Supporting Information:
- Supporting Information S1
- Data Set S1

Correspondence to:
A. Campion,
acampion@alumni.princeton.edu

Citation:
Campion, A., Maloof, A., Schoene, B., Oleynik, S., Sanz-López, J., Blanco-Ferrera, S., . . . Fernández, L. P. (2018). Constraining the timing and amplitude of early Serpukhovian Glacioeustasy with a continuous carbonate record in northern Spain. *Geochemistry, Geophysics, Geosystems*, *19*. https://doi.org/10.1029/2017GC007369

Received 5 DEC 2017
Accepted 5 MAY 2018
Accepted article online 25 MAY 2018

Abstract During the Late Paleozoic Ice Age (LPIA, 345–260 Ma), an expansion of ice house conditions at ~330 Ma caused a nearly synchronous, global unconformity. Subaerially exposed paleotropical carbonates were dissolved by meteoric waters, mixed with the light terrestrial carbon, and recrystallized with over-printed, diagenetic $\delta^{13}C$ values. In Northern Spain, the development of a rapidly subsiding foreland basin kept local sea level relatively high, allowing continuous carbonate deposition to record $\delta^{13}C$ without meteoric overprint. The Spanish sections show a 2‰ increase in $\delta^{13}C$ that can be modeled as the ocean's response to the creation of a significant light carbon sink through widespread meteoric diagenesis of marine carbonates during the near-global hiatus. About 15–35 m of sea level fall would have exposed a large enough volume of carbonate to account for the positive excursion in $\delta^{13}C$ of oceanic DIC. Combining the $\delta^{13}C$ data with high resolution biostratigraphy and new ID-TIMS U-Pb zircon ages from interbedded tuffs, we calculate that the depositional hiatus and glacioeustatic fall caused by the early Serpukhovian phase of ice growth lasted for approximately 3.5 My.

1. Introduction

The icehouse conditions of the Late Paleozoic Ice Age (LPIA) offer an ancient analog to the modern glacial period that began with the Cenozoic ice expansion ~30 Ma and evolved into the interglacial-glacial cycles of the Plio-Pleistocene. As an era with drastically different initial tectonic, biologic, and ocean-atmosphere boundary conditions, the LPIA presents an opportunity to explore how Earth systems' internal feedback mechanisms respond to external climate forcing.

Although originally described as one long, protracted period of Gondwanan glaciation (Heckel, 1986; Veevers & Powell, 1987; Wanless & Shepard, 1936), more detailed chronostratigraphy and precise global correlations of stratigraphic records reveal the LPIA to have been a dynamic, multiphase glaciation with several unique centers of ice growth (Fielding et al., 2008b; Gulbranson et al., 2010; Isbell et al., 2012; Montañez & Poulsen, 2013). Near-field evidence of glaciation, consisting of the physical remains of glaciers including dropstones, striated pavements, and tills, first appears as localized patches in the low-latitude alpine areas of Peru, Bolivia, and the Appalachian Basin in the latest Devonian and early Tournasian (~350 Ma) (Brezinski et al., 2008; Caputo et al., 2008; Isaacson et al., 2008). After 20 My of relatively warmth (Isbell et al., 2003; Rygel et al., 2008), glaciation reinitiates at several discrete ice centers during the early Visean (~345 Ma). Ice growth expands from centers in Argentina (Gulbranson et al., 2010), Australia (Fielding et al., 2008a), and South Africa (Isbell et al., 2008a) with no direct evidence of ice covering Antarctica on the south pole (Isbell et al., 2008b). Despite a potential period of glacial retreat in the Early Pennsylvanian (Henry et al., 2010), peak ice extent was reached again through the Middle Pennsylvanian (Gulbranson et al., 2010).

Following this peak in glaciation, the Middle to Late Pennsylvanian is thought to have been dominated by ~9 My of overall glacial retreat (Frank et al., 2008; Isbell et al., 2012), modulated by potentially orbitally paced, shorter-term fluctuations in ice volume (Belt et al., 2010; Birgenheier et al., 2009; Cecil et al., 2014; Davydov et al., 2010; Eros et al., 2012; Goldhammer et al., 1989; Heckel, 2008; Joeckel, 1999). Evidence of small-scale glacial fluctuation comes from the far-field record, which consists of a repeating hierarchy of

Geochemistry, Geophysics, Geosystems 10.1029/2017GC007369

lithologies. Cyclic packages of rocks from Europe and North America long have been interpreted as recording glacioeustatic change and used to estimate the timing and magnitude of glacial advances and retreats (Fielding & Frank, 2015; Heckel, 1986, 1994; Wanless & Shepard, 1936; West et al., 1997).

The largest and final peak of the LPIA occur in the latest Pennsylvanian to early Permian (~303 Ma) when vast areas of Gondwana are covered in ice sheets (Fielding et al., 2008a; Martin et al., 2008; Montañez & Poulsen, 2013; Rocha-Campos et al., 2008; Stollhofen et al., 2008). This glacial peak includes evidence of glaciation in Antarctica (Isbell et al., 2008b) and at the North Pole (Raymond & Metz, 2004). Warming and deglaciation begin at ~290 Ma and continue through the Permian (Lopez-Gamundi & Buatois, 2010), leaving Earth nearly free of ice until the middle of the Cenozoic.

Several tectonic and biologic factors have been considered as causes of LPIA glaciation (see review in Montañez and Poulsen, 2013). The closure of the Rheic Ocean would have altered ocean circulation by eliminating the subequatorial current, forcing precipitation toward the poles, and potentially causing ice accumulation (Saltzman, 2003; Veevers & Powell, 1987). Continental drift of Gondwana over the South Pole could help explain the shift in ice centers through time (Eyles, 1993; Fielding et al., 2008b; Isbell et al., 2012). Changes in atmospheric circulation and ocean upwelling patterns have not been explored in great detail, but cold coastal upwelling could have prolonged local glaciation in Eastern Australia through the Middle Permian despite a warming world (Jones et al., 2006). Each of these hypotheses can help explain certain aspects of the LPIA, but climate models suggest that none of them can completely explain the glaciation without a drop in atmospheric CO_2 to allow temperatures low enough for ice accumulation (Crowley & Baum, 1992; Montañez & Poulsen, 2013).

The LPIA is roughly coincident with the evolution of vascular land plants, which could have drawn down atmospheric CO_2 through photosynthesis (Algeo et al., 1995; Berner, 1997; Cleal & Thomas, 2005; Eyles, 1993). Vascular land plants also would have increased continental weathering sensitivity by breaking up bedrock and increasing soil acidity (Berner, 1997). However, the major phase of ice growth in the late Visean to early Serpukhovian slightly predates the large-scale lycopsid forest growth of the Bashkirian (~322 Ma) (Cleal & Thomas, 2005), which raises a question of causality. Did the exposure of continental shelves due to glacially driven sea level fall give plants an environment to colonize, thus stimulating an expansion of the terrestrial biosphere? Or did forest growth lower atmospheric pCO_2 enough to drive temperatures down, causing glacial expansion and sea level fall? Around the same time, the formation of Pangea and widespread continental uplift could have changed the sensitivity of silicate weathering rates to pCO_2, potentially exacerbating the drawdown of CO_2 as has been proposed for the effect of the Himalaya on Cenozoic cooling (Broecker & Sanyal, 1998; Garzione, 2008; Walker et al., 1981). Establishing a precise timeline with estimates of ice volume and eustatic change is essential to understanding the relationship between biologically or tectonically driven changes in paleoclimatic factors such as pCO_2 that spurred the onset of the LPIA.

1.1. Studying Paleoclimate With $\delta^{13}C$

Paleovalues of organic carbon burial, carbon sequestration, and atmospheric oxygen are inferred from $\delta^{13}C$ of oceanic DIC using models that couple the governing chemical reactions of the carbon cycle with the known effects of biologic carbon fractionation (Berner, 1999; Kump & Arthur, 1999). Not only are these modeled estimates of such paleoenvironmental parameters dependent on the fidelity of the $\delta^{13}C$ of oceanic DIC record, but they also are dependent on the ability of carbon box models to accurately describe the sources and sinks of the global carbon cycle (e.g., Kump & Arthur, 1999).

Dyer et al. (2015) proposed the need to augment the canonical carbon box model described by Kump and Arthur (1999) to accurately capture the Carboniferous carbon cycle. Before the Mesozoic evolution of calcareous plankton, pelagic carbonate precipitation on shelves represented a much larger percentage of carbon burial during the Carboniferous (Brown et al., 2004). Tropical carbonate platform area during the Visean-Serpukhovian ice expansion was roughly 28× greater than the carbonate platform area we have today (Opdyke & Wilkinson, 1988). Dyer et al. (2015) argued that the subaerial exposure of such vast carbonate platforms would have trapped enough terrestrial carbon through meteoric diagenesis so as to affect the $\delta^{13}C$ of oceanic DIC and thus the paleoenvironmental values estimated from the $\delta^{13}C$ record. We test Dyer et al. (2015)'s hypothesis with a $\delta^{13}C$ record from carbonates that largely avoided meteoric diagenesis to determine if such an effect is possible.

J_ID: GGGE Customer A_ID: GGGE21592 Cadmus Art: GGGE21592 Ed. Ref. No.: 2017GC007369 Date: 7-June-18 Stage: Page: 3

AGU100 ADVANCING EARTH AND SPACE SCIENCE

Geochemistry, Geophysics, Geosystems

10.1029/2017GC007369

1.2. The Carboniferous δ^{13}C Record

The negative δ^{13}C excursions in paleotropical carbonate platforms around the world during the mid to late Visean (~345–330 Ma) go from +5‰ to −8‰ (Figure 1a). These negative excursions are accompanied by karstic exposure surfaces and recrystallization textures in the Western US (Bishop et al., 2009; Dyer et al., 2015). Contemporaneous unconformities in carbonate shelves in the UK, China, North Africa, and the Ural Mountains indicate a global depositional hiatus, within available age constraints (Saunders & Ramsbottom, 1986). A similar top-negative δ^{13}C excursion is observed in Pleistocene carbonates from the Bahamas and is explained by the same mechanism of subaerial exposure and meteoric diagenesis (Swart & Eberli, 2005).

The notable exceptions to this diagenetic signal are the positive δ^{13}C excursions observed in the Donets and Moscow basins from carefully screened, pristine brachiopod shells (Bruckschen et al., 1999), as well as whole rock carbonates from Spain (Buggisch et al., 2008). Earlier records from European brachiopods also show a +3‰ δ^{13}C excursion (Popp et al., 1986). North American data do not reveal as large of a positive excursion, leading Grossman et al. (1993) to posit that a persistent offset of δ^{13}C of oceanic DIC formed between the North American and European oceans due to a change in ocean circulation caused by the formation of Pangea. However, upon analyzing more North American samples, Mii et al. (1999) concluded that there was in fact a 1.5‰ positive δ^{13}C excursion present in pristine North American brachiopods thought to record values of oceanic DIC.

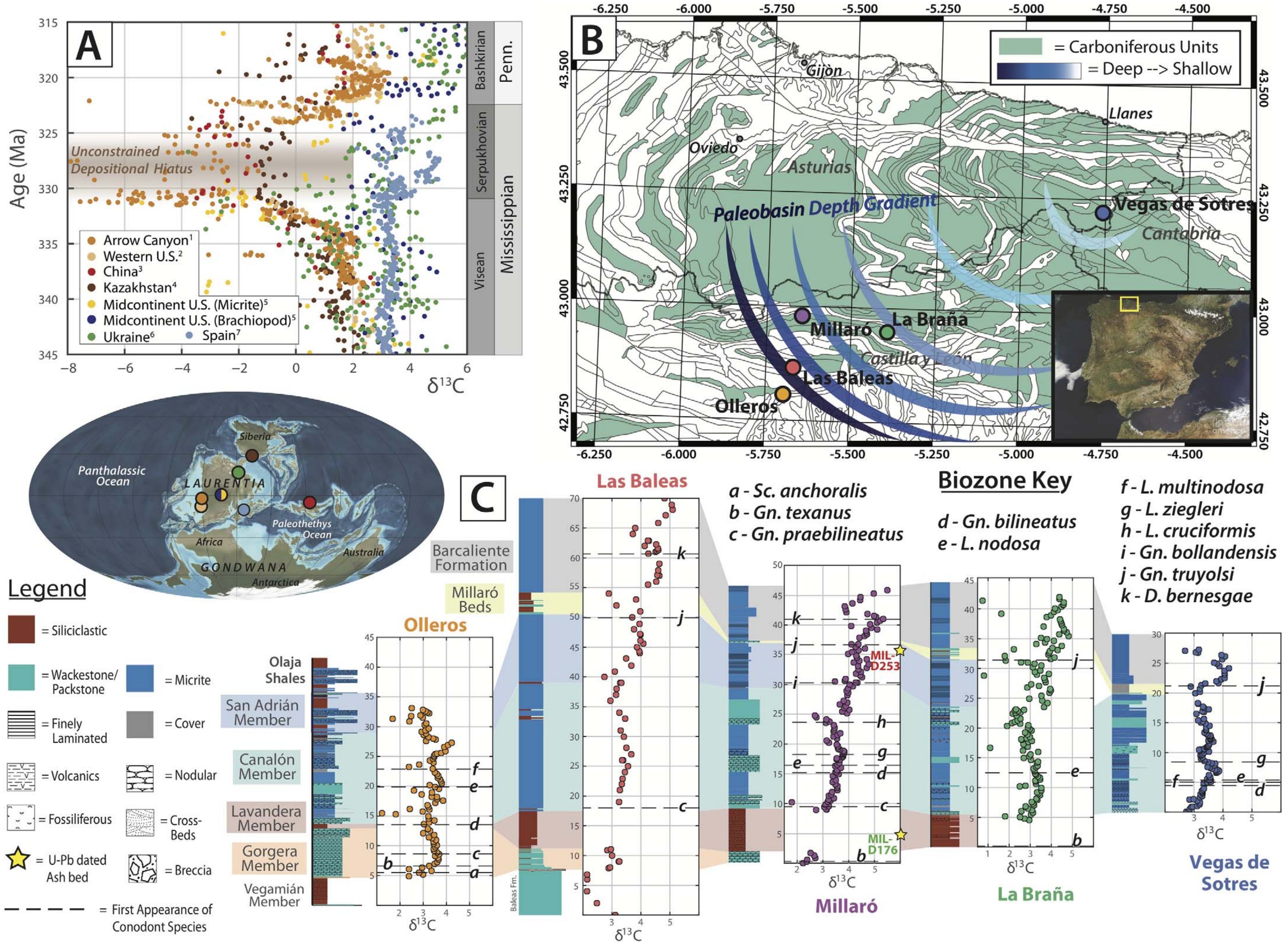

Figure 1. (a) δ^{13}C data from (1) Dyer et al. (2015), (2) Saltzman (2003), (3) Zhao and Zheng (2014), (4) Ronchi et al. (2010), (5) Mii et al. (1999), (6) Bruckschen et al. (1999), and (7) Buggisch et al. (2008), reported relative to VPBD. (b) Stratigraphic section locations in Spain with the paleodepth gradient of the basin adapted from Weil et al. (2013). (c) The Spanish sections with lithologic units, conodont biozones, ash beds, and δ^{13}C values from this study.

ID: kannanb Time: 13:40 I Path: //chenas03/Cenpro/ApplicationFiles/Journals/Wiley/GGGE/Vol00000/180104/Comp/APPFile/JW-GGGE180104

AGU 100 ADVANCING EARTH AND SPACE SCIENCE

Geochemistry, Geophysics, Geosystems 10.1029/2017GC007369

Regardless of the magnitude difference between European and North American samples, an increase in $\delta^{13}C$ of oceanic DIC most commonly is attributed to an increased organic fraction of total carbon burial (*forg*) (Hayes et al., 1999; Kump & Arthur, 1999; Mii et al., 1999). Kump and Arthur (1999) explored other causes, showing that increasing inorganic carbonate weathering relative to organic carbonate and silicate weathering as well as increasing the magnitude of the fractionation effect of organic carbon burial by increasing pCO_2 also can account for a positive excursion of $\delta^{13}C$. More recently Dyer et al. (2015) offered the alternative hypothesis of increased meteoric diagenesis, which we explore in this study.

1.3. Carbon Box Model

The model employed here makes the steady state assumptions that the ocean is well-mixed and that the ocean and atmosphere are in equilibrium. As shown in Figure 2, the inputs into the carbon system include F_v (volcanic outgassing), $F_{w,carb}$ (continental weathering), and $F_{w,org}$ (organic carbon weathering). Each source has a corresponding δ value that is its characteristic isotopic ratio of C^{12} to C^{13}. Carbon from these source reservoirs enters the ocean-atmosphere system and mix together. The relative magnitude of each flux determines the isotopic composition of oceanic DIC and atmospheric pCO_2. Carbon exits the ocean and atmosphere through two sinks: $F_{b,carb}$ (inorganic carbonate burial) and $F_{b,org}$ (organic carbon burial). In the model, $F_{b,carb}$ is buried with a δ value equal to that of DIC. $F_{b,org}$ is buried with a δ value that is a function of DIC, but undergoes a fractionation effect equal to Δ_B

$$\begin{aligned}\frac{dM\delta}{dt} &= F_v\delta_v + F_{w,carb}\delta_{w,carb} + (F_{w,org} - F_R)\delta_{w,org} + F_D\delta_D \\ &- (F_{b,carb} - F_R + F_D)\delta_{DIC} - F_{b,org}(\delta_{DIC} + \Delta_B)\end{aligned} \tag{1}$$

Because inorganic carbon precipitates without significant isotopic fractionation, $\delta^{13}C$ values preserved in pristine marine carbonates are interpreted to reflect oceanic DIC through the geologic record. This assumption simplifies the large amount of variability in platform carbonate $\delta^{13}C$ seen during some epochs and discussed further in section 4.2. The fractionation effect of organic carbon burial, Δ_B, buries carbon $\sim$25‰ more negative than oceanic DIC. If a larger fraction of total oceanic carbon is buried as organic carbon (i.e., if *forg* increases), then more light carbon is taken out of the system, leaving the $\delta^{13}C$ value of oceanic DIC relatively heavier. Thus increasing *forg* commonly is invoked to explain positive $\delta^{13}C$ excursions in carbonate rocks.

With the proposed addition of meteoric diagenesis as a significant light carbon sink (Figure 2), Dyer et al. (2015) introduced an alternative hypothesis for positive excursions of $\delta^{13}C$ of oceanic DIC. Isotopically light carbon from terrestrial systems, dissolved in meteoric waters, mixes with isotopically heavy marine carbonate rock. The resultant dissolved carbon that enters the ocean has a much heavier isotopic signature than the original meteoric water. If the volume of carbonates exposed to meteoric diagenesis is large enough

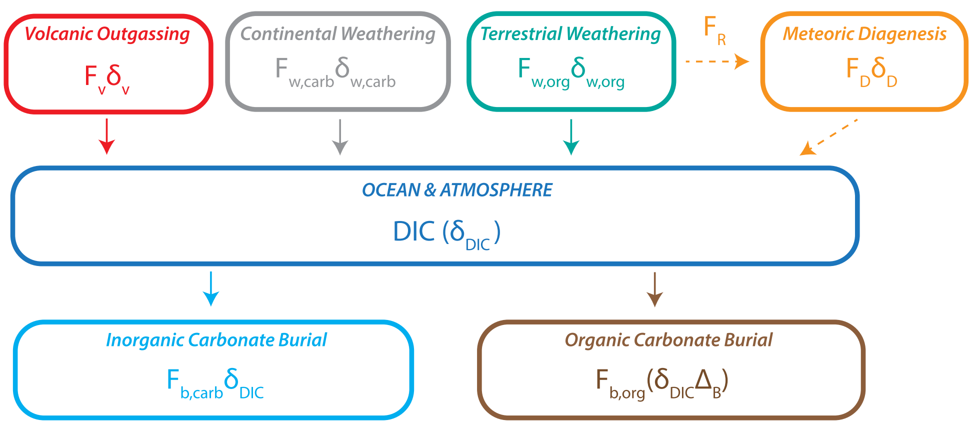

Figure 2. A diagram of a simple one ocean-atmosphere box model of the carbon cycle from Kump and Arthur (1999), with the addition of meteoric diagenesis (Dyer et al., 2015). The one-box model makes the steady state assumptions that the ocean is well-mixed and that the ocean and atmosphere are in equilibrium.

Geochemistry, Geophysics, Geosystems 10.1029/2017GC007369

and the flux is significant to the isotopic mass balance of the global carbon cycle, then the $\delta^{13}C$ of oceanic DIC would increase.

The effect of meteoric diagenesis proposed by Dyer et al. (2015) is captured by F_R (Figure 2 and equation (1)), a flux of organic carbon that instead of entering the ocean-atmosphere box directly, is diverted to react with subaerially exposed carbonate rocks. F_D is the flux of carbonate material from the platforms that is dissolved and enters the ocean-atmosphere box. F_R and F_D balance each other such that if $F_R > F_D$ there is net dissolution of the carbonate platforms, as would be evidenced in the geologic record by karsting, caves, and dissolution-collapse breccia.

To maintain isotopic equilibrium, the change in the global isotopic C^{12}/C^{13} ratio through time is assumed to be zero ($\frac{dM\delta}{dt}=0$). With assumed values for carbon fluxes and their respective isotopic values, and an estimate for δ_{DIC}, equation (1) can be solved for F_R to estimate the magnitude of the meteoric flux.

2. Geologic Background

The Cantabrian Zone in Northern Spain contains sedimentary rocks deposited in a foreland basin that formed as the Rheic Ocean closed during the Variscan Orogeny (Matte, 2001; Weil et al., 2013). During the Mississippian, as the basin subsided due to the approaching load of Laurentia, flexural subsidence outpaced any global sea level fall, leading to laterally monotonous sedimentation over wide areas of the basin (Martínez Catalán et al., 2003; Pérez-Estaún et al., 1994). Because Laurentia approached from the west, the foreland basin was deeper in the west and shallower in the east (Figure 1b). Due to this depth gradient of the basin, the carbonates of the Alba Formation contain abundant shallower-water foraminifera in the northeast and deeper-water conodont species in the southwest (Cózar et al., 2016; Sanz-López et al., 2007).

The Alba Formation contains deep water carbonates deposited atop a drowned marine platform that spans preorogenic and synorogenic periods (García-López & Sanz-López, 2002; Sanz-López et al., 2007). The first three members, the Lavandera, Gorgera, and Canalón, are highly condensed as a slow rate of deposition persisted from the late-Tournasian through the late Visean. These units mostly are composed of red, nodular, crinoidal wackestone with some tabular, red-grey micrite (Figure 1c). Atop the initial three members, the deepening of the basin and onset of synorogenic deposition caused the lithologic transition to the dark grey, laminated micrite unit known as the San Adrián Member and basinal shales of the Olaja Shale.

In the southwestern region most proximal to the orogenic front, the Olaja Shale is interrupted by the arrival of the oldest synorogenic siliciclastic turbidites called the Olleros Formation (Olleros section, Figure 1c). In the other sections farther from the orogenic front, the deepening basin allows for continued carbonate sedimentation. The San Adrián member is capped by a thin, extremely fossiliferous, green wackestone known as the Millaró Beds. After the Millaró Beds, the sections transition into hundreds of meters of black limestone micrite with fine laminations with very high sedimentation rates called the Barcaliente Formation.

Carbon isotopes range from 3‰ to 5‰ and there is no lithological evidence of subaerial exposure or meteoric alteration such as mudcracks, karsting, or plant roots. Interbedded in the carbonate stratigraphy are volcanic ash beds, offering the opportunity to radiometrically constrain the timing of the $\delta^{13}C$ record in Spain and to calibrate the global $\delta^{13}C$ record using biostratigraphic correlations.

3. Results

3.1. CA-ID-TIMS U-Pb

Nine zircon grains from two ash samples from the Millaró section were chosen for ID-TIMS U-Pb geochronology following the methods outlined in Samperton et al. (2015). All analyses were made on single zircon grains via isotope dilution, using the EARTHTIME (^{202}Pb)-^{205}Pb-^{233}U-^{235}U (ET2535) tracer solution with isotopic ratios measured on an Isotopx Phoenix62 thermal ionization mass spectrometer (TIMS). A full U-Pb data table has been uploaded as a supporting information (ds01) and the full methodology description are included in the supporting information (S1).

MIL-D176 was taken from the Lavandera Mb in the Millaró section. (Figure 1c). Six grains were concordant and clustered in a 1 million year age range (338.5–339.5 Ma) while two grains were discordant, falling on a discordia with an upper intercept of ~575 Ma (Figure 3). Of the six younger concordant grains, the F3

AGU 100 ADVANCING EARTH AND SPACE SCIENCE

Geochemistry, Geophysics, Geosystems

10.1029/2017GC007369

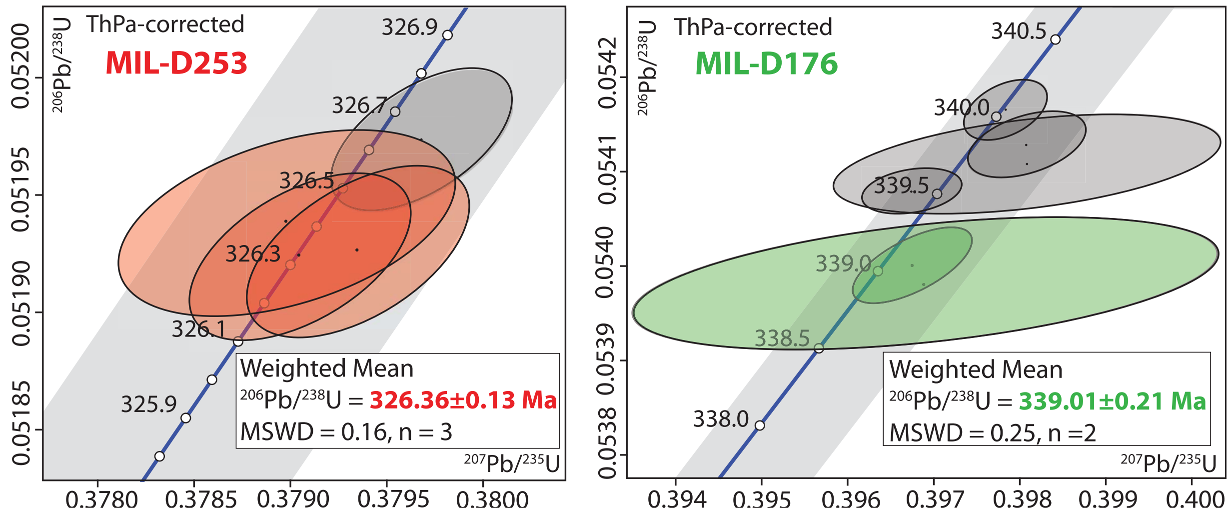

Figure 3. Concordia plots of U-Pb dates from MIL-D176 and MIL-D253 samples. The younger cluster from each sample is interpreted as the age closest to eruption and deposition of the ashfall.

youngest two are interpreted as best representing the age of deposition, with a weighted mean $^{206}Pb/^{238}U$ date for MIL-D176 of 339.01 ± 0.21/0.23/0.43 Ma (MSWD = 0.25). In the reported ±X/Y/Z uncertainties, X corresponds to the internal uncertainty associated with the U-Pb decay system, Y also includes the uncertainty associated with the tracer solution, and Z additionally contains the uncertainty of the decay constant.

In MIL-D253, sampled from the Millaró Beds (Figure 1c), several grains defined a discordia with an upper intercept of ∼1,500 Ma. Out of four younger concordant grains, one was discarded as it fell along the mixing line between the upper intercept and the younger ages and had increased the MSWD from 0.16 to 2.0. We report the weighted mean $^{206}Pb/^{238}U$ date of the three youngest grains of 326.26 ± 0.13/0.16/0.38 Ma, as the best estimate of the age of deposition (Figure 3).

3.2. Carbon Isotopes

Carbonate hand samples were taken at 0.3–0.5 m resolution in each stratigraphic section (Figure 1). In the lab, the samples were slabbed, polished, and drilled for powder. Micrite was targeted during drilling, while calcite veins, grains, and shell fragments were carefully avoided. Powders were loaded into borosilicate reaction vials, heated to 110°C to remove water, then reacted with five drops of H_3PO_4 at 72°C. The CO_2 analyte was then measured with a Sercon IRMS coupled with a GasBench II sampling device at Princeton University. Results are reported relative to the Vienna Pee Dee Belemnite (VPBD) standard and have a measurement accuracy of ±0.1‰.

Spanish $\delta^{13}C$ values range from +3‰ to 5‰, recording a drastically different signal that that of Arrow Canyon (Figure 5). $\delta^{13}C$ does vary across the Spanish basin indicating environmental and/or diagenetic differences between the distal and proximal portions of the basin (Figures 1c and 5). The $\delta^{13}C$ records of Millaró, Vegas de Sotres, and Las Baleas (Figure 5) agree at the base of the sections with values ranging from 3‰ to 4‰. Further up in the section, at the first appearance of *Lochriea ziegleri* at ∼332.2 Ma (Figure 5), the records diverge as a gradient develops across the basin. The shallower Vegas de Sotres section remains around +3.2‰ while the deeper Millaró and Las Baleas sections show a positive excursion to values as high as +5‰ (Figure 5).

4. Discussion

4.1. Age Model

Two simplifying assumptions were made to create the age model: (1) sedimentation rate is constant in the Millaró section between horizons with ages, and (2) first appearances of conodont zones across the Cantabrian Zone are synchronous. First appearances in all the Spanish sections were correlated with the first appearances in the Millaró section following García-López and Sanz-López (2002), Sanz-López et al. (2004,

AGU 100 ADVANCING EARTH AND SPACE SCIENCE

Geochemistry, Geophysics, Geosystems

10.1029/2017GC007369

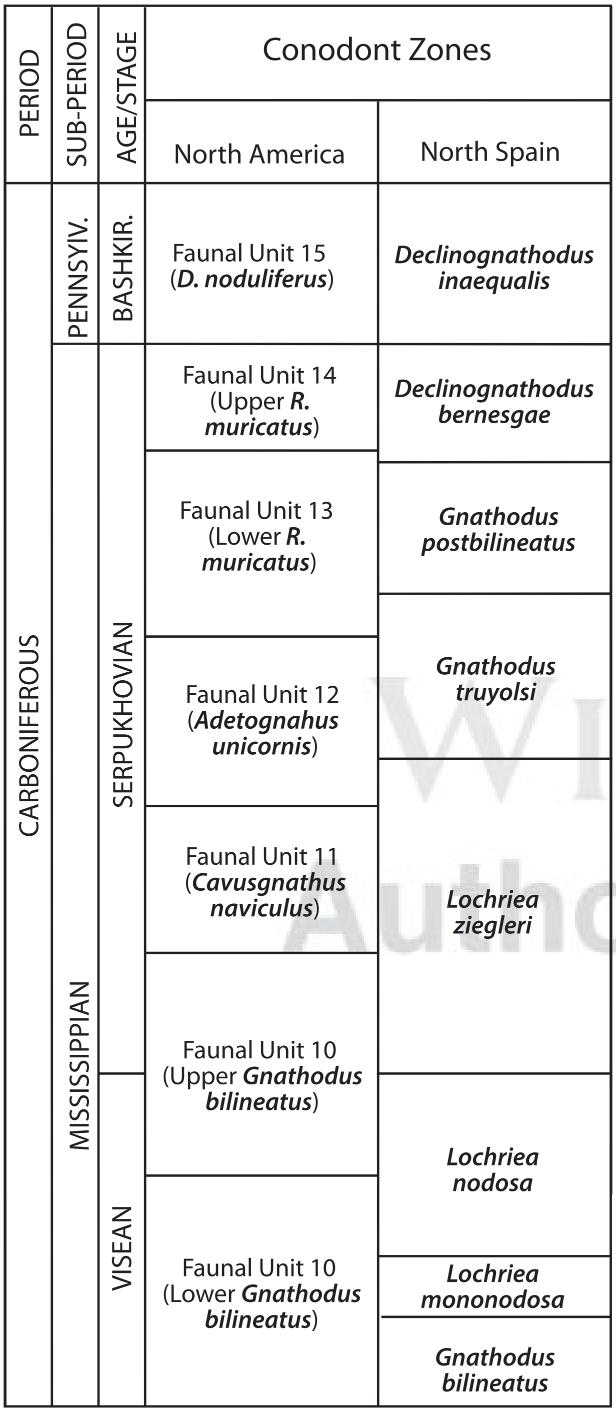

Figure 4. The chronostratigraphic correlation of the Faunal Units at Arrow Canyon to the conodont zones in the Cantabrian basin. Correlations were determined by first appearances of conodonts and foraminifera from Lane and Brenckle (2005), Kulagina et al. (2008), Bishop et al. (2009), Davydov et al. (2012), Sanz-López and Blanco-Ferrera (2013), and Sanz-López et al. (2013).

2006, 2007), Sanz-López and Blanco-Ferrera (2012), and Cózar et al. (2016). The conodont species defining the Faunal Units in Arrow Canyon were chronostratigraphically correlated to the Spanish sections using first appearances of conodonts and foraminifera. A synthesis of biostratigraphic data from Lane and Brenckle (2005), Kulagina et al. (2008), Bishop et al. (2009), Davydov et al. (2012), Sanz-López and Blanco-Ferrera (2013), and Sanz-López et al. (2013) used in this study is illustrated in Figure 4.

Millaró was selected as the reference section because it has the most precise documentation of first appearances of conodont species and ash beds. The two U-Pb dates from the Millaró section reported in this work, as well as a 332.5 $\pm$ 0.07 Ma date from the Belgium (Pointon et al., 2014) and a 333.87 $\pm$ 0.08 Ma date from the Ural Mountains (Schmitz & Davydov, 2012), were used to construct the age model. The two existing dates were chosen because the reported biostratigraphy allowed the dates to be correlated to the Millaró section with $\pm$1 m accuracy. The ash bed the Schmitz and Davydov (2012) date was sampled from occurs before the first appearance of *L. nodosa* while the Pointon et al. (2014) date was sampled from between the first appearances of *Lochriea nodosa* and *L. ziegleri*. Uniform sedimentation rates were assigned between each dated horizon in the Millaró section. First appearance tie points from other sections then were assigned dates based on the age of that first appearance in the Millaró section. In each section, a uniform sedimentation rate was calculated between each tie point, resulting in a continuous age model for each section (Figure 5).

Correlating the Spanish sections with Arrow Canyon allows us to apply the Spanish age model we calibrate here to the Arrow Canyon section, which contains no radiometric ages itself. Calculating the duration of the depositional hiatus at Arrow Canyon has implications for the rate and magnitude of glacial expansion and sea level fall during that time. Based on our correlations, the first occurrence of *L. ziegleri*, which is currently considered to be indicative of the Visean-Serpukhovian boundary (Davydov et al., 2012; Richards, 2011), occurs before the depositional hiatus at Arrow Canyon. Past estimates of the boundary range from 326.4 Ma (Gradstein et al., 2004) to 328.3 Ma (Heckel, 2008) to 330.9 Ma (Davydov et al., 2012). Our age model estimates the first appearance of *L. ziegleri* to be 332.2 Ma (Figure 5), considerably earlier than past estimates. Based the stratigraphic relationships observed in our data and the estimated age model, we consider the hiatus at Arrow Canyon and corresponding positive $\delta^{13}C$ excursion in the Spanish sections to occur in the early Serpukhovian.

While Figure 5 shows the age model calculated using the most likely stratigraphic placements of dates, there is uncertainty associated with each age placement and correlation. Considering these uncertainties has a measurable impact on our estimate of the hiatus at Arrow Canyon and thus the duration of early Serpukhovian glacial expansion. To quantify the full range of possible durations of the hiatus, we consider the uncertainty for each age placement. The samples from the Millaró section were taken with $\pm$0.1 m uncertainty while the dates from the literature were correlated within $\pm$1 m and $\pm$0.4 for the 333.87 $\pm$ 0.08 and 332.50 $\pm$ 0.07 dates, respectively. Probability distributions were assigned to each date based on its associated placement uncertainty and then the age model was calculated 10,000 times, drawing randomly from the distributions for each date for each iteration. The beginning

AGU 100 ADVANCING EARTH AND SPACE SCIENCE

Geochemistry, Geophysics, Geosystems 10.1029/2017GC007369

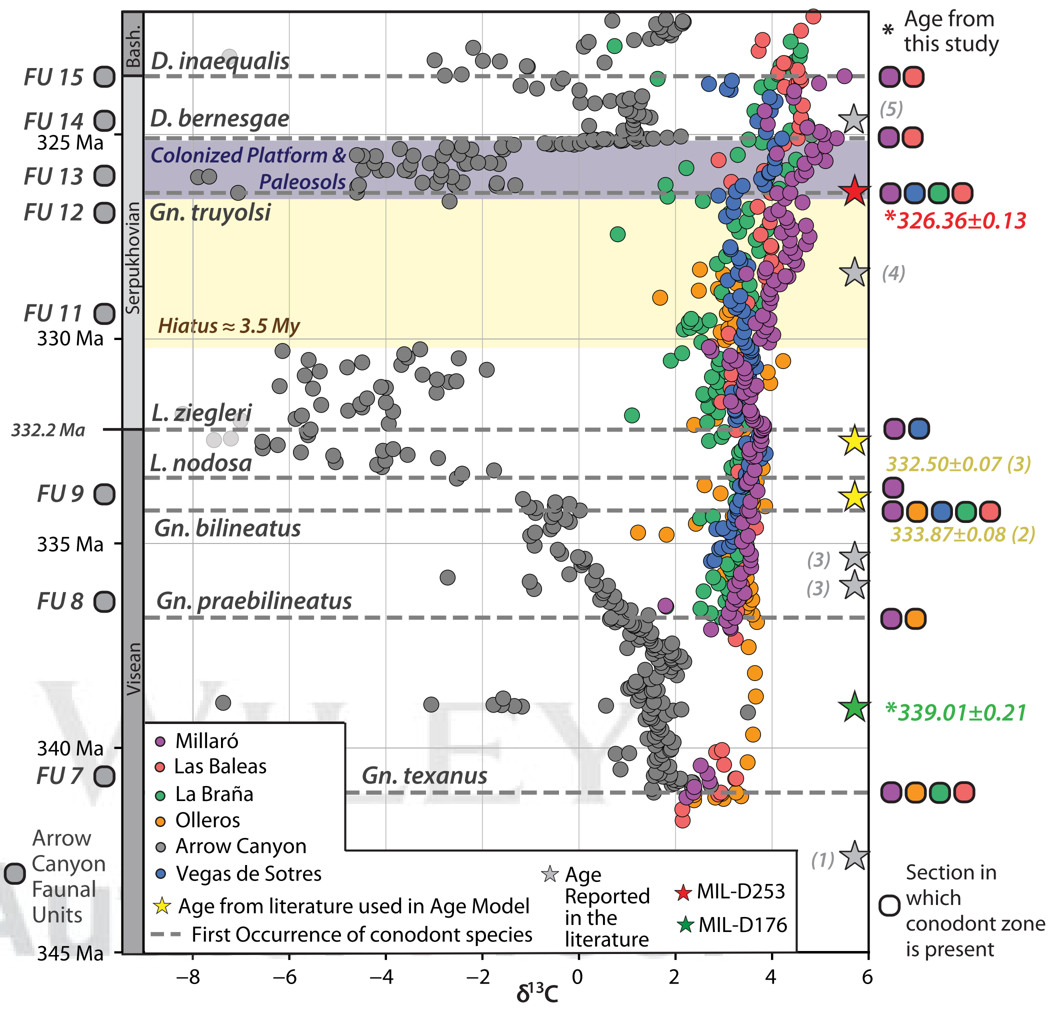

Figure 5. Spanish sections from this study with Arrow Canyon (Dyer et al., 2015) correlated chronostratigraphically and plotted with our new age model. Dates are from (1) Davydov et al. (2010), (2) Schmitz and Davydov (2012), (3) Pointon et al. (2014), (4) Davydov et al. (2010), and (5) Pointon et al. (2012). The lower boundary of the Serpukhovian is located at the first occurrence of conodont *L. ziegleri*.

of the hiatus is dated to 330.2 ± 0.6 Ma, while the end of the hiatus is 326.6 ± 0.1 Ma. Therefore, the hiatus is estimated to be 3.5 ± 0.3 My. Error bounds reflect ±2 standard deviations of the calculated distributions.

Additional uncertainty in the model is attributed to the unknown amount of subaerial erosion associated with the major exposure event, which ensures that the beginning of the hiatus is placed at the earliest point of its possible range. The end of the hiatus is marked at the first bed of carbonate after the major exposure surface and hiatus at Arrow Canyon. However, just following the period defined as a hiatus, there are roughly 60 m of interbedded paleosols, siliciclastics, thin limestones with roots, exposure surfaces, and gaps in the sedimentation at Arrow Canyon (Bishop et al., 2009; Dyer et al., 2015). Alternations in sedimentation and subaerial exposure indicate small-scale fluctuations in sea level during this interval, accompanied by negative δ^{13}C values as highlighted in Figure 5. It is unclear how global sea level would have been behaving during this period of interbedded colonized carbonate platforms and paleosols. Continuous carbonate sedimentation did not begin until after this interval, making the precise end of the hiatus difficult to determine. Due to such sources of error, 3.5 ± 0.3 My is most likely a minimum estimate of the hiatus at Arrow Canyon and is our best estimate of the mid-Carboniferous global hiatus, although such estimates could be replicated for other sections in the future given adequate biostratigraphic correlations.

Geochemistry, Geophysics, Geosystems 10.1029/2017GC007369

4.2. Intrabasinal δ^{13}C Variability

Stratigraphic variability of δ^{13}C in shallow water carbonates through the geologic record often have been interpreted as reflecting global changes in oceanic DIC (Saltzman, 2003; Vahrenkamp, 1996). However, recent studies of modern carbonate platforms suggest that such variability can be dominated by local platform dynamics. Swart and Eberli (2005) measure a 4‰ difference between the ^{13}C-enriched aragonite produced by green algae on the Great Bahama Bank platform (+5‰) compared to the lighter periplatform carbonates dominated by calcite from coccoliths and foraminifera (+1‰). Swart and Eberli (2005) suggest that δ^{13}C variability through time could be attributed to the mixing between calcite and aragonite end-members, with changes in the volume of aragonite exported down the slope affecting the δ^{13}C recorded in periplatform sediments. It also is possible that the variation in percent aragonite in such sediments could be due to temporal variability in the dynamics of early marine diagenesis (Higgins et al., 2018). These local effects that cause deviation in δ^{13}C from global DIC vary geographically over the past 10 million years (Swart, 2008), and may have been more or less important in the Carboniferous world.

In either the syn-deposition or post-deposition cases, the mineralogical difference between the aragonite and calcite end-members might only account for a ~1‰ of the isotopic gradient (Emrich et al., 1970). The remainder of the 4‰ difference measured by Swart and Eberli (2005) could be due to increased photosynthesis and evaporation selectively removing light carbon from restricted, shallow water carbonate shelves, leaving shelf sediments even heavier (Lloyd, 1964). However, in the opposite direction, effusion of CO_2 into alkaline waters during rapid photosynthesis can cause depletion of δ^{13}C and result in low δ^{13}C of local DIC (Lazar & Erez, 1992). δ^{13}C data from carbonate platforms are complicated and can be influenced by local phenomena, so we do not exclude the possibility that part of the +2‰ excursion recorded in the Millaró section in Spain is due to changes to periplatform carbonate generation that do not reflect changes in global ocean DIC.

During the period of time that corresponds to the hiatus at Arrow Canyon, we observe the deeper Millaró section to have δ^{13}C values ~2‰ heavier than the shallow Vegas de Sotres section, seemingly opposite to the pattern expected for Swart and Eberli (2005)-style aragonite export from the shelf. A gradient in which outer shelf sections are carbon isotopically heavier than inner shelf sections is observed in the modern Florida platform. Patterson and Walter (1994) posits that isotopically light terrestrial water flows into the shallow end of the platform and mixes with ocean water, resulting in lighter δ^{13}C values in the shallow carbonate sections. Because the shallow waters are somewhat restricted, the freshwater does not mix with the deeper water, meaning the deeper carbonate sections record heaver δ^{13}C closer to oceanic DIC. Glacioeustatic fall during the early Serpukhovian could have caused the Cantabrian basin to become restricted and less well-mixed, allowing a carbon isotope gradient to develop across the basin. Thus we interpret the positive δ^{13}C excursion signal from Millaró as the most likely to record a signal of global DIC during the Visean-Serpukhovian. The three deepest sections (Millaró, La Braña, and Las Baleas) each record positive excursions of 1.5–2.5‰ during the hiatus at Arrow Canyon (Figure 5), and we proceed with the assumption that at least part of this signal reflects changes in global DIC.

4.3. Sea Level Fall

The box model outlined in Figure 2 can simulate a scenario in which a positive ~2‰ δ^{13}C excursion in oceanic DIC is caused entirely by the effect of exposed carbonate platforms acting as a light carbon sink through the process of meteoric diagenesis. F_R is output in units of 10^{12} mol C/ky, which can be converted to a volume of carbonate per ky using the molar mass of carbon (N) and the density of carbonate (ρ). The volume of carbon ($\frac{F_R * N}{\rho}$) is then divided by the total area of rock and the percent rock replaced to isolate the depth of diagenesis (d) (equation (2)). If diagenetic depth is controlled entirely by subaerial exposure due to glacioeustasy, d can be interpreted as a measure of changing average global sea level

$$d = \frac{\left(\frac{F_R * N}{\rho}\right)}{PA * per} \tag{2}$$

Estimates from Kump and Arthur (1999) of the various carbon reservoir sizes and characteristic isotopic signatures (Table 1) were used in the model. *forg*, calculated as $\frac{F_{b,org}}{F_{b,org}+F_{b,carb}}$, is set to 0.20 by Kump and Arthur (1999), which initializes $\delta^{13}C_{DIC}$ to be 0‰. Because $\delta^{13}C_{DIC}$ at the base of the Spanish section is 2‰, *forg* was initialized as 0.24 in this model so as to correctly output 2‰ as initial δ^{13}C of oceanic DIC. The δ^{13}C record T1

AGU 100 ADVANCING EARTH AND SPACE SCIENCE

Geochemistry, Geophysics, Geosystems

10.1029/2017GC007369

Table 1
*Carbon Fluxes and Isotopic Signatures Used in this Study (*Kump and Arthur, 1999*)*

	Flux (mol $\times$ 10^{12}/kyr)	δ^{13}C (‰)
Sources		
Volcanic outgassing (F_{volc})	6,000	-5
Continental weathering ($F_{w,carb}$)	40,000	0
Terrestrial organic weathering ($F_{w,org}$)	10,000	-22
Meteoric diagenesis (F_R)	F_R	2
Sinks		
Inorganic carbonate burial ($F_{b,carb}$)	38,000	δ_{DIC}
Organic carbonate burial ($F_{b,org}$)	12,000	$\delta_{DIC}-\Delta_B$
forg	0.24	

from Millaró, as our best estimate of oceanic DIC, was input as δ_{DIC}. An average global area of carbonate platforms reported by Walker et al. (2002) of 39 $\times$ 10^6 km^2 and a range of percent marine carbonate replacement during meteoric diagenesis estimated by Dyer et al. (2015) of 12–19% were used.

The output of the model (Figure 6) compares the light carbon sink solution to the traditional increased organic carbon burial scenario, each of which could explain the positive excursion observed in the Spanish δ^{13}C signal. Our results show that, when $\Delta_B = -29‰$, *forg* must increase from 0.24 to ~0.32, which means increasing organic carbon burial by 4,800 $\times$ 10^{12} g/kyr. When the fractionation effect (Δ_B) is smaller in magnitude, organic carbon is buried at heavier values meaning a larger volume must be buried to account for the positive δ^{13}C excursion recorded in the Spanish sections. When $\Delta_B = -25‰$, *forg* must reach values of ~0.36.

Simply changing Δ_B while holding *forg* constant could theoretically account for changes in $\delta^{13}C_{DIC}$. While it is difficult to model through geologic time, Δ_B is a function of pCO_2 and growth rate. Increasing pCO_2 causes an increase in the magnitude of Δ_B, with a plateau of $-33‰$ at very high concentrations of pCO_2 (Kump & Arthur, 1999). To account for the positive anomaly in δ^{13}C observed in Spain, Δ_B would have to reach unrealistic values less than $-40‰$. Furthermore, pCO_2 is expected to be decreasing during this period of cooling to estimated values of 420–840 ppmv (Horton et al., 2010), which would correspond to Δ_B values greater than $-30‰$ (Kump & Arthur, 1999).

Drastically increasing *forg* results in geochemical models estimating very high levels of atmospheric oxygen. Organic carbon normally decomposes when it reacts with O_2, reducing the carbon, and releasing CO_2. When that carbon is buried before it can fully decompose, O_2 concentration increases (Berner, 1999). The amount of organic carbon burial required to explain the positive $\delta^{13}C_{DIC}$ anomaly results in an extreme rise in atmospheric oxygen to concentrations of 30%, compared to 21% today (Berner, 2006). Such high concentrations of O_2 would invoke a strong negative feedback that would cause fires to destroy the terrestrial plant ecosystem (Belcher et al., 2010). These extreme oxygen predictions could be reduced to more reasonable levels if the marine carbon isotopic record is not only a function of *forg*, but also of global meteoric diagenesis.

If meteoric diagenesis alone explains the positive excursion in δ^{13}C, the model requires a 15–35 m sea level fall (Figure 6). The estimate is very sensitive to the percent volume carbonate that is replaced by diagenesis, with a lower value of *per* = 5% resulting in ~70 m of sea level change. New observations from meteorically

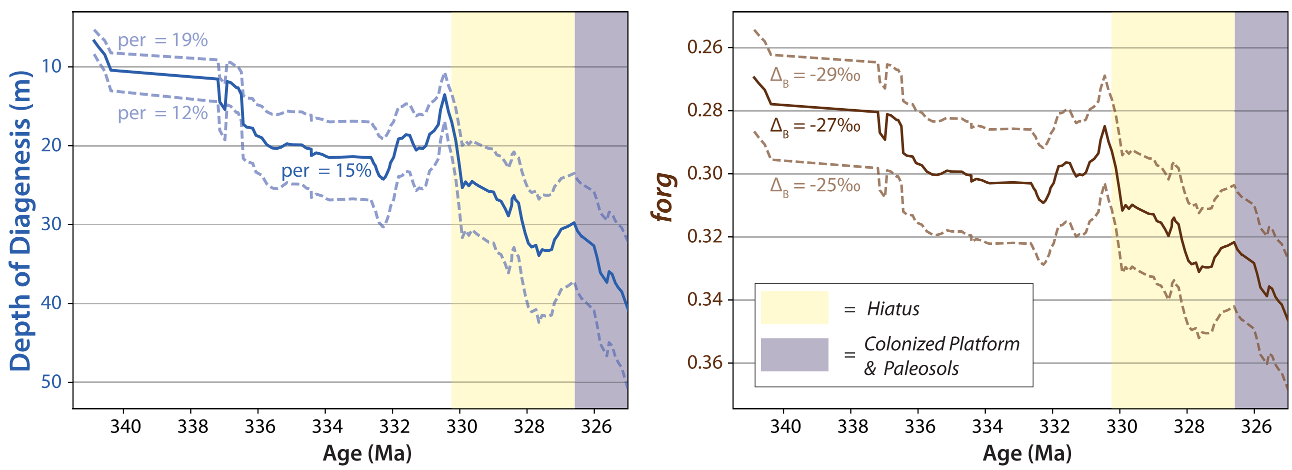

Figure 6. The depth of diagenesis required to create the δ^{13}C signal from Millaró using a range of possible values (12–19%) for the percent of exposed platform replaced with light meteoric carbon. Data from Millaró was input using a 5 point moving average to reduce the effect of outliers. For the left plot, $\Delta_B = -0.29$. The right plot shows the corresponding change in *forg* required to create the same signal.

altered Visean-Serupukhovian platform carbonates would help constrain the model output. Similarly, the sea level estimate fluctuates with the isotopic composition of the exposed carbonate platforms, estimated to be 2‰ in our model. If the isotopic composition of the carbonate entering the ocean through meteoric diagenesis is in fact lower due to oxidized organic matter on the exposed platforms, then a larger amount of sea level fall would be required to account for the positive excursion of oceanic $\delta^{13}C$. The trajectory of projected sea level fall suggests that sea level continued to fall throughout the period of intermittent sedimentation at Arrow Canyon directly following the hiatus. Smaller-scale ice growth and resultant sea level fluctuations during this time could have allowed periodic sedimentation.

While changes in sea level as estimated from far-field records have varied between 10 and 200 m (Rygel et al., 2008), more recent studies have estimated smaller values between 20 and 70 m (Dyer et al., 2015; Fielding & Frank, 2015; Montañez & Poulsen, 2013; Waters & Condon, 2012). Following the ice-sheet model from Horton et al. (2010), 15–35 m of sea level change corresponds to ~560 ppmv pCO_2 and 6–15 $\times$ 10^6 km^3 of ice volume, which is less than the maximum extent of 20 $\times$ 10^6 km^3 estimated from the near-field record (Montañez & Poulsen, 2013). For comparison, there are slightly larger estimates for the initial growth of the Cenozoic ice sheet during a major cooling phase at the Eocene-Oligocene boundary of 55 m sea level change corresponding to a 25 $\times$ 10^6 km^3 ice sheet (Miller et al., 2009).

In reality, it is likely that the $\delta^{13}C$ signal observed in Spain recorded the interaction between several forces: increased organic carbon burial rates, changes in platform aragonite export, local early marine diagenesis, and global meteoric diagenesis. Disentangling each mechanism from the $\delta^{13}C$ record would require additional data and analysis of complementary isotopic systems from rocks around the world. Invoking the global meteoric diagenesis lever as at least part of the cause of the positive $\delta^{13}C$ excursion in the early Serpukhovian, rather than only increased *forg*, resolves the timeline with the evolution of vascular land plants, reconciles the amount of atmospheric oxygen estimated by geochemical models, and requires a 15–35 m fall in sea level over 3.5 My that is consistent with other estimations.

5. Conclusion

A fully integrated data set of carbonate $\delta^{13}C$, biostratigraphic correlations of conodont first appearances, and U-Pb zircon dates from volcanic ashes in northern Spain suggest that oceanic DIC reached its highest values precisely when shallow marine carbonate platforms around the world were subaerially exposed and diagenetically altered. If the $\delta^{13}C$ increase of ~2‰ in Spanish carbonates reflects primary DIC and is, in fact, the direct result of meteoric alteration of exposed carbonates due to glacioeustasy, then we estimate ~15–35 m of sea level fall during glacial expansion in the early Serpukhovian. Based on our new U-Pb dates and biostratigraphic correlations, this hiatus due to glacioeustatic fall lasted for 3.5 My before glacial expansion reversed or began fluctuating such that sedimentation could begin again.

Acknowledgments
Funding for this study was provided for two years of senior thesis research by funding agencies at Princeton University, including the Princeton Environmental Institute, the Smith-Newton Family, ODOC, and the Geoscience Department at Princeton. Project CGL2013-44458-P of the Ministerio de Ciencia y Tecnología of Spain and FEDER funding from the European Community also contributed. JS-L and SB-F benefited from support via the project CGL2016-78738 of the Spanish Ministerio de Economía y Competitividad. This work was made possible by Blake Dyer's previous work, support, and guidance. Thanks to Jas Raczinski for assistance in the field and Artemis Eeyster, Ari Zuaro, Sam Gwizd, and Alex Hager for preparing samples for stable isotope analysis. Kyle Samperton managed the lab work for all the zircon analyses. CA-ID-TIMS U-Pb data are available in the supporting information file online. Code and data used to construct the age model and produce Figure 3, including the new and compiled $\delta^{13}C$ data used in this study, are available at https://github.com/alison-campion/biostrat-age-model.

References

Algeo, J. T., Berner, R. A., Maynard, J. B., & Scheckler, S. E. (1995). Late Devonian Oceanic anoxic events and biotic crises: "Rooted" in the evolution of vascular land plants? *GSA Today*, *5*(3), 60–65.

Belcher, C. M., Yearsley, J. M., Hadden, R. M., McElwain, J. C., & Rein, G. (2010). Baseline intrinsic flammability of Earth's ecosystems estimated paleoatmospheric oxygen over the past 350 million years. *Proceedings of the National Academy of Sciences of the Unites States of America*, *107*(52), 22448–22453.

Belt, E. S., Heckel, P. H., Lentz, L. J., Bragonier, W. A., & Lyons, T. W. (2010). Record of glacial-eustatic sea-level fluctuations in complex middle to late Pennsylvanian facies in the Northern Appalachian Basin and relation to similar events in the Midcontinent basin. *Sedimentary Geology*, *238*(1–2), 79–100.

Berner, R. A. (1997). The rise of plants and their effect on weathering and atmospheric CO_2. *Science*, *276*(5312), 544–546.

Berner, R. A. (1999). Atmospheric oxygen over Phanerozoic time. *Proceedings of the National Academy of Sciences of the Unites States of America*, *96*(20), 10955–10957.

Berner, R. A. (2006). GEOCARBSULF: A combined model for Phanerozoic atmospheric O_2 and CO_2. *Geochimica et Cosmochimica Acta*, *70*(23), 5653–5664.

Birgenheier, L. P., Fielding, C. R., Rygel, M. C., Frank, T. D., & Roberts, J. (2009). Evidence for dynamic climate changes on sub-10^6-year scales from the late Paleozoic glacial record, Tamworth Belt, New South Wales. *Australia Journal of Sedimentary Research*, *79*(2), 56–82.

Bishop, J. W., Montañez, I. P., Gulbranson, E. L., & Brenckle, P. L. (2009). The onset of mid-Carboniferous glacio-eustasy: Sedimentologic and diagenetic constrains, Arrow Canyon, Nevada. *Palaeogeography, Palaeoclimatology, Palaeoecology*, *276*(1–4), 217–243.

Brezinski, D. K., Cecil, C. B., Skema, V. W., & Stamm, R. (2008). Late Devonian glacial deposits from the eastern United States signal an end of the mid-Paleozoic warm period. *Palaeogeography, Palaeoclimatology, Palaeoecology*, *268*(3–4), 143–151.

Broecker, W. S., & Sanyal, A. (1998). Does atmospheric CO_2 police the rate of chemical weathering? *Global Biogeochemical Cycles*, *12*(3), 403–408.

AGU 100 ADVANCING EARTH AND SPACE SCIENCE

Geochemistry, Geophysics, Geosystems 10.1029/2017GC007369

Brown, P. R., Lees, J. A., & Young, J. R. (2004). Calcareous nanoplankton evolution and diversity through time. In Thierstein, H. R. & Young, J. R. (Eds.), *Coccolithophores: From molecular processes to global impact* (pp. 481–508). Berlin, Germany: Springer.

Bruckschen, P., Oesmann, S., & Veizer, J. (1999). Isotope stratigraphy of the European Carboniferous: Proxy for ocean chemistry, climate and tectonics. *Chemical Geology*, *161*(1–3), 127–163.

Buggisch, W., Joachimski, M. M., Sevastopulo, G., & Morrow, J. R. (2008). Mississippian δ^{13}C*carb* and conodont apatite δ^{18}O records—Their relation to the Late Paleozoic glaciation. *Palaeogeography, Palaeoclimatology, Palaeoecology*, *268*(3–4), 273–282.

Caputo, M. V., Gonçalves de Melo, J. H., Steel, M., & Isbell, J. L. (2008). Late Devonian and early Carboniferous glacial records of South America. *Geological Society of America Special Paper*, *441*, 161–174.

Cecil, C. B., DiMichele, W. A., & Elrick, S. D. (2014). Middle to Late Pennsylvanian cyclothems, American Midcontinent: Ice-age environmental changes and terrestrial biotic dynamics. *Comptes Rendus Geoscience*, *346*(7–8), 159–168.

Cleal, C. J., & Thomas, B. A. (2005). Paleozoic tropical rainforests and their effect on global climates: Is the past the key to the present? *Geobiology*, *3*(1), 13–31.

Cózar, P., Somerville, I. D., Sanz-López, J., & Blanco-Ferrera, S. (2016). Foraminiferal biostratigraphy across the Visean/Serpukhovian boundary in the Vegas de Sotres section (Cantabrian Mountains, Spain). *Journal of Foraminiferal Research*, *46*(2), 171–192.

Crowley, T. J., & Baum, S. K. (1992). Modeling late Paleozoic glaciation. *Geology*, *20*(6), 507–510.

Davydov, V. I., Crowley, J. L., Schmitz, M. D., & Poletaev, V. I. (2010). High-precision U-Pb zircon age calibration of the global Carboniferous time scale and Milankovitch band cyclicity in the Donets Basin, eastern Ukraine. *Geochemistry Geophysics Geosystems*, *11*, Q0AA04. https://doi.org/10.1029/2009GC002736

Davydov, V. I., Korn, D., & Schmitz, M. D. (2012). The carboniferous period. In Gradstein, F. M., Ogg, J. G., Schmitz, M. D., & Ogg, G. M. (Eds.), *The geologic time scale 2012* (Vol. 2, pp. 603–651). Oxford, UK: Elsevier.

Dyer, B., Maloof, A., & Higgins, J. A. (2015). Glacioeustasy, meteoric diagenesis, and the carbon cycle during the mid-Carboniferous. *Geochemistry, Geophysics, Geosystems*, *10*, 3383–3399. https://doi.org/10.1002/2015GC006002

Emrich, K., Ehhalt, D. H., & Vogel, J. C. (1970). Carbon isotopic fractionation during the precipitation of calcium carbonate. *Earth and Planetary Science Letters*, *8*(5), 363–371.

Eros, J. M., Montañez, I. P., Osleger, D. A., Davydov, V. I., Nemyrovska, T. I., Poletaev, V. I., et al. (2012). Sequence stratigraphy and onlap history of the Donets Basin, Ukraine: Insight into Carboniferous icehouse dynamics. *Palaeogeography, Palaeoclimatology, Palaeoecology*, *313–314*, 1–25.

Eyles, N. (1993). Earth's glacial record and its tectonic setting. *Earth-Science Reviews*, *35*(1–2), 1–248.

Falkowski, P. G., Katz, M. E., Knoll, A. H., Quigg, A., Raven, J. A., Schofield, O., et al. (2004). The evolution of modern eukaryotic phytoplankton. *Science*, *305*(5682), 354–360. AQ3

Fielding, C. R., & Frank, T. D. (2015). Onset of the glacioeustatic signal recording Late Palaeozoic Gondwanan ice growth: New data from palaeotropical East Fife, Scotland. *Palaeogeography, Palaeoclimatology, Palaeoecology*, *426*, 121–138.

Fielding, C. R., Frank, T. D., Birgenheier, L. P., Rygel, M. C., Jones, A. T., & Roberts, J. (2008). Stratigraphic imprint of the Late Paleozoic Ice Age in eastern Australia: A record of alternating glacial and non-glacial climate regime. *Journal of Geological Society London*, *165*(1), 129–140.

Fielding, C. R., Frank, T. D., & Isbell, J. L. (2008). The Late Paleozoic Ice Age—A review of current understanding and synthesis of global climate parameters. *Geological Society of America Special Paper*, *441*, 1–12.

Frank, T. D., Birgenheier, L. P., Montañez, I. P., Fielding, C. R., & Rygel, M. C. (2008). Late Paleozoic climate dynamics revealed by comparison of ice-proximal stratigraphic and ice-distal isotopic records. *Geological Society of America Special Paper*, *441*, 121–138.

García-López, S., & Sanz-López, J. (2002). Devonian to lower Carboniferous conodont biostratigraphy of the Bernesga Valley section (Cantabrian Zone, NW Spain). In García-López, S. & Bastida, F. (Eds.), *Palaeozoic conodonts from northern Spain* (pp. 163–205). Madrid, Spain: Cuadernos del Museo Geominero, 1, Instituto Geológico y Minero de España.

Garzione, C. N. (2008). Surface uplift of Tibet and Cenozoic global cooling. *Geology*, *36*(12), 1003–1004.

Goldhammer, R. K., Oswald, E. J., & Dunn, P. A. (1989). The hierarchy of stratigraphic forcing—An example from Middle Pennsylvanian (Desmoinesian) shelf carbonates of the southwestern Paradox basin, Honaker Trail, Utah, *Kansas Geologic Survey, Subsurface Geology*, *12*, 27–30.

Gradstein, F. M., Ogg, J. G., & Smith, A. G. (2004). *A geologic time scale*. Cambridge, UK: Cambridge University Press. https://doi.org/10.1017/CBO9780511536045

Grossman, E. L., Mii, H., & Yancey, T. E. (1993). Stable isotopes in Late Pennsylvanian brachiopods from the United States: Implications for Carboniferous paleoceanography. *Geologic Society of America Bulletin*, *105*(10), 1284–1296.

Gulbranson, E. L., Montanez, I. P., Schmitz, M. D., Limarino, C. O., Isbell, J. L., Marenssi, S. A., et al. (2010). High-precision U-Pb calibration of Carboniferous glaciation and climate history, NW Argentina. *Geologic Society of America Bulletin*, *122*(9–10), 1480–1498.

Hayes, J. M., Strauss, H., & Kaufman, A. J. (1999). The abundance of ^{13}C in marine organic matter and isotopic fractionation in the global biogeochemical cycle of carbon during the past 800 Ma. *Chemical Geology*, *161*(1–3), 103–125.

Heckel, P. H. (1986). Sea-level curve for Pennsylvanian eustatic marine transgressive-regressive cycles along midcontinent outcrop belt, North America. *Geology*, *14*(4), 330–334.

Heckel, P. H. (1994). Evaluation of evidence for glacio-eustatic control over marine Pennsylvanian cyclothems in North America and consideration of possible tectonic effects. In Dennison, M. & Ettensohn, F. R. (Eds.), *Concepts in sedimentology paleontology, Tectonic and eustatic controls on sedimentary cycles* (Vol. 4). Tulsa, OK: Society of Sedimentary Geology.

Heckel, P. H. (2008). Pennsylvanian cyclothems in Midcontinent North America as far-field effects of waxing and waning of Gondwana ice sheets. *Geological Society of America Special Paper*, *441*, 275–289.

Henry, L. C., Isbell, J. L., Limarino, C. O., McHenry, L. J., & Fraiser, M. L. (2010). Mid-Carboniferous deglaciation of the Protoprecordillera, Argentina, recorded in the Agua de Jagüel paleovalley. *Palaeogeography, Palaeoclimatology, Palaeoecology*, *298*(1–2), 112–129.

Higgins, J. A., Blättler, C. L., Lundstrom, E. A., Santiago-Ramos, D. P., Akhtar, A. A., Crüger Ahm, A.-S., et al. (2018). Mineralogy, early marine diagenesis, and the chemistry of shallow-water carbonate sediments. *Geochimica et Cosmochimica Acta*, *220*, 512–534. https://doi.org/10.1016/j.gca.2017.09.046

Horton, D. E., Poulsen, J. C., & Pollard, D. (2010). Influence of high-latitude vegetation feedbacks on late Paleozoic glacial cycles. *Nature Geosciences*, *3*(8), 572–334.

Isaacson, P., Diaz-Martinez, E., Grader, G., Kalvoda, J., Babek, O., & Devuyst, F. (2008). Late Devonian-earliest Mississippian glaciation in Gondwanaland and its biogeographic consequences. *Palaeogeography, Palaeoclimatology, Palaeoecology*, *268*(3–4), 126–142.

Isbell, J. L., Cole, D. I., & Catuneanu, O. (2008). Carboniferous-Permian glaciation in the main Karoo Basin, South Africa: Stratigraphy depositional controls, and glacial dynamics. *Geological Society of America Special Paper*, *441*, 71–82.

AGU 100 ADVANCING EARTH AND SPACE SCIENCE

Geochemistry, Geophysics, Geosystems 10.1029/2017GC007369

Isbell, J. L., Henry, L. C., Gulbranson, E. L., Limarino, C. O., Fraiser, M. L., Koch, Z. J., et al. (2012). Glacial paradoxes during the Late Paleozoic Ice Age: Evaluating the equilibrium as a control on glaciation. *Gondwana Research*, *22*(1), 1–19.

Isbell, J. L., Koch, Z. J., Szablewski, G. M., & Lenaker, P. A. (2008). Permian glacigenic deposits in the Transantarctic Mountains, Antarctica. *Geological Society of America Special Paper*, *441*, 5–24.

Isbell, J. L., Miller, M. F., Wolfe, K. L., & Lenaker, P. A. (2003). Timing of late Paleozoic glaciation in Gondwana: Was glaciation responsible for the development of northern hemisphere cyclothems? *Geological Society of America Special Paper*, *370*, 5–24.

Joeckel, R. M. (1999). Paleosol in Galesburg Formation (Kansas City Group, Upper Pennsylvanian), northern Midcontinent, USA: Evidence for climate change and mechanisms of marine transgression. *Journal of Sedimentary Research*, *69*(3), 720–737.

Jones, A. T., Frank, T. D., & Fielding, C. R. (2006). Cold climate in the eastern Australian mid to late Permian may reflect cold upwelling waters. *Palaeogeography, Palaeoclimatology, Palaeoecology*, *237*(2–4), 370–377.

Kulagina, E. I., Gibshman, N. B., & Nikolaeva, S. V. (2008). Foraminifera-based correlation of the Chesterian Stage in the Mississippian type region, Illinois, USA with the Serpukhovian Stage of Russia. *Newsletter on Carboniferous Stratigraphy*, *26*, 14–18.

Kump, L. R., & Arthur, M. A. (1999). Interpreting carbon-isotope excursions: Carbonates and organic matter. *Chemical Geology*, *161*(1–3), 181–198.

Lane, R. H., & Brenckle, P. L. (2005). Stratigraphy and biostratigraphy of the Mississippian subsystem (Carboniferous system) in its type region, the Mississippi River Valley of Illinois, Missouri and Iowa. In Heckel, P. H. (Ed.), *Type Mississippian subdivisions and biostratigraphic succession* (Vol. 34, pp. 76–105). Champaign, IL: Illinois State Geological Survey.

Lazar, B., & Erez, J. (1992). Carbon geochemistry of marine-derived brines: I. ^{13}C depletions due to intense photosynthesis. *Geochimica et Cosmochimica Acta*, *56*(1), 335–345.

Lloyd, M. R. (1964). Variations in the oxygen and carbon isotope ratios of Florida Bay mollusks and their environmental significance. *The Journal of Geology*, *72*(1), 84–111.

Lopez-Gamundi, O. R., & Buatois, L. A. (Eds.) (2010). Late Paleozoic Glacial Events and Postglacial Transgressions in Gondwana. In *Geologic Society of America Special Publication* (Vol. 468, pp. 1–207). Boulder, CO: Geologic Society of America.

Martin, J. R., Redfern, J., & Aitken, J. F. (2008). A regional overview of the late Paleozoic glaciation in Oman. In *Resolving the Late Paleozoic Ice Age in time and space, special paper of the Geological Society of America* (Vol. 441, pp. 83–96). Boulder, CO: Geologic Society of America.

Martínez Catalán, J. R., Arenas, R., & Díez Balda, M. A., (2003). Large extensional structures of developed emplacement of a crystalline thrust sheet: The Mondonedo nappe (NW Spain). *Journal of Structural Geology*, *25*(11), 1815–1839.

Matte, P. (2001). The Variscan collage and orogeny (480–290 ma) and the tectonic definition of the Armorica microplace: A review. *Terra Nova*, *13*(2), 122–128.

Mii, H., Grossman, E. L., & Yancey, T. E. (1999). Carboniferous isotope stratigraphies of North America: Implications for Carboniferous paleoceanography and Mississippian glaciation. *Geologic Society of America Bulletin*, *111*(7), 960–973.

Miller, K. G., Wright, J. D., Katz, M. E., Wade, B. S., Browning, J. V., Cramer, B. S., et al. (2009). Climate threshold at the Eocene-Oligocene transition: Antarctic ice sheet influence on ocean circulation. In Koeberl, C. & Montanari, A. (Eds.), *The Late Eocene Earth—Hothouse, icehouse, and impacts* (Geol. Soc. of Am. Bull. Spec. Pap. 452). Boulder, CO: Geologic Society of America.

Montañez, I. P., & Poulsen, C. J. (2013). The Late Paleozoic Ice Age: An evolving paradigm. *Annual Review of Earth and Planetary Sciences*, *41*(1), 629–656.

Opdyke, B. N., & Wilkinson, B. H. (1988). Surface area control of shallow cratonic to deep marine carbonate accumulation. *Paleoceanography*, *3*(6), 685–703.

Patterson, W. P., & Walter, L. M. (1994). Depletion of ^{13}C in seawater CO_2 on modern carbonate platforms: Significance for the carbon isotopic record of carbonates. *Geology*, *22*(10), 885–888.

Pérez-Estaún, A., Pulgar, J., Banda, E., & Alvarez-Marrón, J. (1994). Crustal structure of the external variscides in northwest Spain from deep seismic reflection profiling. *Tectonophysics*, *232*(1–4), 91–118.

Pointon, M., Chew, D., Ovtcharova, M., Sevastopulo, G., & Crowley, Q. (2012). New high-precision U-Pb dates from western European Carboniferous tuffs: Implications for time scale calibration, the periodicity of late Carboniferous cycles and stratigraphic correlation. *Geological Society of London*, *169*(6), 713–721.

Pointon, M., Chew, D., Ovtcharova, M., Sevastopulo, G., & Delcambre, B. (2014). High-precision U-Pb zircon CA-ID-TIMS dates from western European Carboniferous late Visean bentonites. *Geological Society of London*, *171*(5), 649–658.

Popp, B. N., Anderson, T. F., & Sandberg, P. A. (1986). Brachiopods as indicators of original isotopic compositions in some Paleozoic limestones. *Geological Society of America Bulletin*, *97*(10), 1262–1269.

Raymond, A., & Metz, C. (2004). Ice and its consequences: Glaciation in the Late Ordovician, Late Devonian, Pennsylvanian-Permian, and Cenozoic compared. *Journal of Geology*, *112*(6), 655–670.

Richards, B. C. (2011). Report of the task group to establish a GSSP close to the existing Viséan-Serpukhovian boundary. *Newsletter on Carboniferous Stratigraphy*, *29*, 26–29.

Rocha-Campos, A. C., dos Santos, P. R., & Canuto, J. R. (2008). Late Paleozoic glacial deposits of Brazil: Paraná Basin. In *Resolving the Late Paleozoic Ice Age in time and space, special paper of the Geological Society of America* (Vol. 441, pp. 97–114). Boulder, CO: Geologic Society of America.

Ronchi, P., Ortenzi, A., Borromeo, O., Claps, M., & Zempolich, W. G. (2010). Depositional setting and diagenetic processes and their impact on the reservoir quality in the late Visean-Bashkirian Kashagan carbonate platform (pre-Caspian Basin, Kazakhstan). *AAPG Bulletin*, *94*(9), 1313–1348.

Rygel, M. C., Fielding, C. R., Frank, T. D., & Birgenheier, L. P. (2008). The magnitude of late Paleozoic glacioeustatic fluctuations: A synthesis. *Journal of Sedimentary Research*, *78*(8), 500–511.

Saltzman, M. R. (2003). Late Paleozoic Ice Age: Oceanic gateway of pCO_2. *Geology*, *31*(2), 151–154.

Samperton, K. M., Schoene, B., Cottle, J. M., Keller, C. B., Crowley, J. L., & Schmitz, M. D. (2015). Magma emplacement, differentiation and cooling in the middle crust: Integrated zircon geochronological-geochemical constraints from the Bergell Intrusion, Central Alps. *Chemical Geology*, *417*, 322–340.

Sanz-López, J., & Blanco-Ferrera, S. (2012). Revisión estratigráfica del Misisipiense al Pensilvaniense más bajo de la zona Cantábrica y la posición de los limites entre los pisos. In *Congreso Geológico de España*, Oviedo, 17–19 July 2012 (Geo-Temas 13, pp. 163–166) [CD-ROM]. AQ4

Sanz-López, J., & Blanco-Ferrera, S. (2013). Early evolution of *Declinognathodus* close to the Mid-Carboniferous boundary interval in the Barcaliente type section (Spain). *Palaeontology*, *56*, 927–946.

Sanz-López, J., Blanco-Ferrera, S., & García-López, S. (2004). Taxonomy and evolutionary significance of some *Gnathodus* species (conodonts) from the Mississippian of the Northern Iberian Peninsula. *Revista Española De Micropaleontología*, *36*, 215–230.

Geochemistry, Geophysics, Geosystems 10.1029/2017GC007369

Sanz-López, J., Blanco-Ferrera, S., García-López, S., & Sánchez de Posada, L. C. (2006). The mid-Carboniferous boundary in Northern Spain: Difficulties for correlation of the global stratotype section and point. *Rivista Italiana di Paleontologia e Stratigrafia*, *112*, 3–22.

Sanz-López, J., Blanco-Ferrera, S., García-López, S., & Sánchez de Posada, L. C. (2013). Conodont chronostratigraphical resolution and *Declinognathodus* evolution close to the Mid-Carboniferous Boundary in the Barcaliente Formation type section, NW Spain. *Lethaia*, *46*, 438–453.

Sanz-López, J., Blanco-Ferrera, S., García-López, S., Sánchez de Posada, L. C., & García-López, S. (2007). Serpukhovian conodonts from Northern Spain and their biostratigraphic application. *Palaeontology*, *50*(4), 883–904.

Saunders, W., & Ramsbottom, W. (1986). The mid-Carboniferous eustatic event. *Geology*, *14*(3), 208–212.

Schmitz, M. D., & Davydov, V. I. (2012). Quantitative radiometric and biostratigraphic calibration of the Pennsylvanian-Early Permian (Cisuralian) time scale, and pan-Euramerican chonostratigraphic correlation. *Geological Society of America Bulletin*, *124*(3–4), 549–577.

Stollhofen, H., Werner, M., Stanistreet, I., Armstrong, R., Fielding, C., Frank, T., et al. (2008). Single-zircon U-Pb dating of Carboniferous-Permian tuffs, Namibia, and the intercontinental deglaciation cycle framework. In *Resolving the Late Paleozoic Ice Age in time and space, special paper of the Geological Society of America* (Vol. 441, pp. 83–96). Boulder, CO: Geologic Society of America.

Swart, P. K. (2008). Global synchronous changes in the carbon isotopic composition of carbonate sediments unrelated to changes in the global carbon cycle. *Proceedings of the National Academy of Sciences of the Unites States of America*, *105*(37), 13741–13745.

Swart, P. K., & Eberli, G. (2005). The nature of the δ^{13}C of periplatform sediments: Implications for stratigraphy and global carbon cycle. *Sedimentary Geology*, *175*(1–4), 115–129.

Vahrenkamp, V. C. (1996). Carbon isotope stratigraphy of the Upper Kharaib and Shuaiba Formations: Implications for the Early Cretaceous evolution of the Arabian Gulf region. *American Association of Petroleum Geologists Bulletin*, *80*, 647–662.

Veevers, J., & Powell, C. (1987). Late Paleozoic glacial episodes in Gondwanaland reflected in transgressive-regressive depositional sequences in Euramerica. *Geologic Society of America Bulletin*, *98*(4), 475–487.

Wanless, H. R., & Shepard, F. P. (1936). Sea level and climate changes related to late Paleozoic cycles. *Geological Society of America Bulletin*, *47*(8), 1177–1206.

Walker, J. C., Hays, P. B., & Kasting, J. F. (1981). CA negative feedback mechanism for the long-term stabilization of Earth's surface temperature. *Journal of Geophysical Research*, *86*(C10), 9776–1747.

Walker, L. J., Wilkinson, B. H., & Ivany, L. C. (2002). Continental drift and Phanerozoic carbonate accumulation in shallow-shelf and deep marine settings. *Journal of Geology*, *110*(1), 75–87.

Waters, C. N., & Condon, D. J. (2012). Nature and timing of the late Mississippian to mid-Pennsylvanian glacio-eustatic sea-level changes of the Pennine Basin, UK. *Journal of Geological Society of London*, *169*(1), 37–51.

Weil, A. B., Gutiérrez-Alonso, G., Johnston, S., & Pastor-Galán, D. (2013). Kinematic constraints on buckling a lithospheric-scale orocline along the northern margin of Gondwana: A geologic synthesis. *Tectonophysics*, *582*, 25–49.

West, R. R., Archer, A. W., & Miller, K. B. (1997). The role of climate in stratigraphic patterns exhibited by late Palaeozoic rocks exposed in Kansas. *Palaeogeography, Palaeoclimatology, Palaeoecology*, *128*(1–4), 1–16.

Zhao, M.-Y., & Zheng, Y.-F. (2014). Marine carbonate records of terrigenous input into Paleothethyan seawater: Geochemical constraints from Carboniferous limestones. *Geochimica et Cosmochimica Acta*, *141*, 508–531.